Nanoscale

Article

Periodic oscillation of ion conduction of nanofluidic diodes using a chemical oscillator

Received 00th January 20xx,
Accepted 00th January 20xx

DOI: 10.1039/x0xx00000x

www.rsc.org/

Huacheng Zhang,[a,*] Jue Hou,[a] Ranwen Ou,[a] Yaoxin Hu,[a] Huanting Wang,[a,*] and Lei Jiang[b]

Periodic ion-conduction oscillation of biological ion channels in living system are essential for numerous life processes. Here we report an oscillatory nanofluidic system that can self-regulate its ion-conduction states under constant conditions. The oscillatory nanofluidic system is constructed by integrating a chemical oscillator into artificial single nanochannel system. Oscillating chemical reactions of the pH oscillator carried out inside the nanochannel are used to switch the surface property of the channel between highly and lowly charged states, thus realizing an autonomous, continuous and periodic oscillation of the ion conductance of the channel between high and low ion-conduction states. The ion-conduction switching is characterized by the periodic ion current oscillation of the nanochannel measured under constant conditions. The oscillation period of the nanofluidic devices decreased gradually with increasing the working temperature. This study is a potential step toward the ability to directly convert chemical energy to ion-conduction oscillation in nanofluidics. On the basis of these findings, we believe that a variety of artificial oscillatory nanofluidic systems will be achieved in future by integrating artificial functional nanochannels with diverse oscillating chemical reactions.

Introduction

Smart nanofluidic systems with artificial responsive nanochannels[1-5] have recently drawn enormous research attention because of their potential in mimicking the intelligent stimuli-gated ion transport features of biological ion channels[6] and practical applications in building high-performance nanodevices.[7-10] Since an single artificial conical nanochannel has been proved to show voltage-dependent ion current fluctuations with opening and closing kinetics similar to voltage-gated biological ion channels,[11] scientists from worldwide research groups have further developed a variety of bio-inspired smart stimuli-gated nanochannels, demonstrating diversely biomimetic pH-,[12-22] temperature-,[23-25] light-,[26, 27] voltage-,[28, 29] pressure-,[30] molecule-,[31-35] and ion-responsive[36-39] ion transport properties.[2-4] These artificial functional nanochannel materials have been widely used to build various advanced nanofluidic devices for high-efficient biosensings, logic gates, and energy conversions.[4, 40-42] However, ionic transport in current nanofluidic devices mostly function with on-off switching of external stimuli, construction of nanofluidic systems that can self-regulate their ion transport states under constant conditions will make them more versatile and expand the range of their applications. Furthermore, periodic ion-conduction oscillation of biological ion channels are essential for numerous life processes, many of which are self-oscillated, e.g. the cell cycle, heartbeat and brain waves.[43, 44] These self-oscillation behaviors in living systems are clearly autonomous, continuous, and periodic, which play a very important role in biology.

Inspired by the intelligent biological oscillation functions, research on artificial self-oscillating materials, which could automatically switch between different conformational states under continuously- and constantly-supplied conditions, can provide important information for a better understanding of the self-oscillation mechanisms in biological systems, facilitating the development of useful microfluidic devices in biochemical and pharmaceutical studies.[45, 46] Such as self-oscillating polymers and gels have been developed based on various oscillating chemical reactions and applied to synthetic muscles,[47] biomimetic actuators,[48, 49] autonomous mass transport on surfaces,[50] and periodic drug-delivery devices.[51] Although rapid progress has been made in developing artificial marco/micro-scaled self-oscillating systems in the past decades,[52-55] design of structurally simple yet efficient nanofluidic systems for autonomous and periodic mass transport control on the nanoscale is still in its early stage. Such as an artificial self-gating ion channel system has been recently developed to achieve biomimetic cyclic and periodic gating functions.[56]

In this work, we further construct an oscillatory nanofluidic device to realize continuous and periodic control of the ion conduction of nanofluidic diodes. The nanofluidic device is developed by integrating a chemical oscillator into single bullet-shaped nanochannels. Oscillating chemical reactions of the chemical oscillator carried out inside the nanochannel can drive a cyclical and periodic change of the inner surface property of the nanochannels, and thus leading to the ion conduction oscillation of the nanofluidic device. Ion-current-

[a] Department of Chemical Engineering, Monash University, Clayton, Victoria 3800, Australia. Email: zhanghc@mail.ipc.ac.cn; huacheng.zhang@monash.edu; huanting.wang@monash.edu
[b] Laboratory of Bioinspired Smart Interface Science, Technical Institute of Physics and Chemistry, Chinese Academy of Sciences, Beijing 100190, People's Republic of China.

†Electronic Supplementary Information (ESI) available: Figures S1-S10 and equations S1-S3. See DOI: 10.1039/x0xx00000x

time measurements under constant conditions demonstrate autonomous, continuous, and periodic ion transport properties of the oscillatory nanofluidic devices under the constantly-supplied reacting solution. The ion current oscillation period of the device can be further gradually manipulated by changing the working temperature of the device. As an example in fabricating self-oscillating nanofluidic system, both strategy and experimental results reported in this work provide a versatile avenue to construct novel intelligent nanofluidic oscillators based on various oscillating chemical reactions.

Results and discussion

Single bullet-shaped nanochannels were prepared by asymmetric chemical etching of a 12 μm thick polyethylene terephthalate (PET) membranes containing a single ion track in the centre. The bullet-shaped nanochannel had a small opening on one side (namely tip side) and a large opening on the other side (namely base side), and its radius increased sharply at the tip region. To confirm the geometry of the bullet-shaped nanochannel, a multichannel membrane with a channel density of about 10^8 cm^{-2} was prepared under the same condition as the single-channel membrane and characterized by scanning electron microscopy (SEM). Fig. 1a shows SEM image of the cross section of a bullet-shaped nanochannel embedded within the PET membrane. SEM images of the tip and base sides of the bullet-shaped channels are shown in Fig. S1 in the Supporting Information (ESI). The statistic average radius of the base side is 86 ± 9 nm, while the mean tip radius is 14 ± 3 nm. During the chemical etching process, carboxyl groups were exposed on the channel surface,[57, 58] which rendered the channel a good pH responsive property with p*K*a of ca. 3.8. As illustrated in fig. 1b, current-voltage (I-V) curves of the nanochannel measured in 0.1 M KCl solutions with different pHs demonstrated its pH-responsive ion transport features. The nanochannel showed a linear I-V curve at pH 3, while I-V curves became more and more asymmetric with pH increasing from 4 to 10 (Fig. S2a in ESI). This result is attributed to the gradual deprotonation of the carboxyl groups at high pH conditions, which produced excess negative charges on the inner surface of the nanochannel. For instance, the nanochannel was uncharged at pH 3, partly charged at pH 5, and fully charged at pH 10 (fig. 1c). As a result, the bullet-shaped nanochannel functioned as a nanofluidic diode, and its ion conductance at positive voltages could be described as a function of pH value (Fig. S2b in ESI). Moreover, through systematic testing I-V properties of the nanochannel under symmetric and asymmetric pH conditions, we found that the ion transport property of the bullet-shaped nanochannel was mainly controlled by the surface property of its tip region (Fig. S3 in ESI).

After fabrication and systematic characterization of the nanofluidic diodes, we constructed the oscillatory nanofluidic device by integrating a $NaBrO_3$-Na_2SO_3-$K_4Fe(CN)_6$-H_2SO_4 oscillator into the tip side of the nanochannel. Here, the $NaBrO_3$-Na_2SO_3-$K_4Fe(CN)_6$-H_2SO_4 system was selected as an example of chemical oscillators for building self-oscillating nanofluidic devices because it has high amplitude pH oscillations (pH oscillates between ~3 and ~7) and it is stable in a wide range of experimental parameters.[52, 59] Besides, at this pH range, the nanochannel could undergo reversible surface property changes between highly and lowly charged states, leading to obvious high-low switching of the ion conduction of the nanofluidic diode at positive voltage (Fig. S2b in ESI).

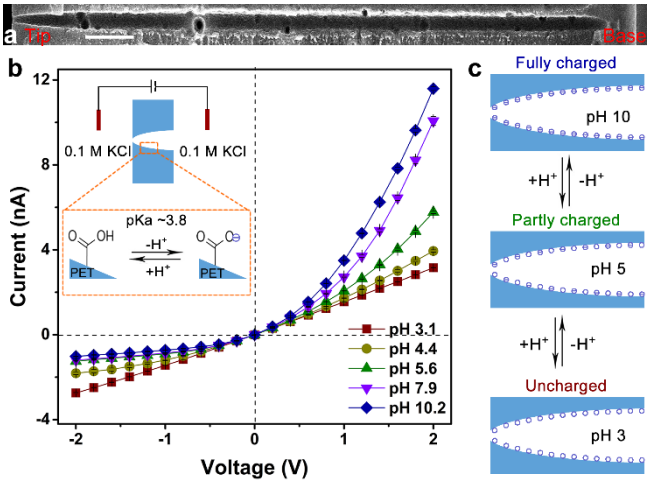

Fig. 1. Nanochannel characterization. (a) SEM image of the cross section of the bullet-shaped nanochannel, scale bar 1 μm. (b) pH-dependent current-voltage curves of the nanochannel measured in 0.1 M KCl solutions of different pHs from 3 to 10. (c) Effect of pH on the surface charge density of the nanochannel.

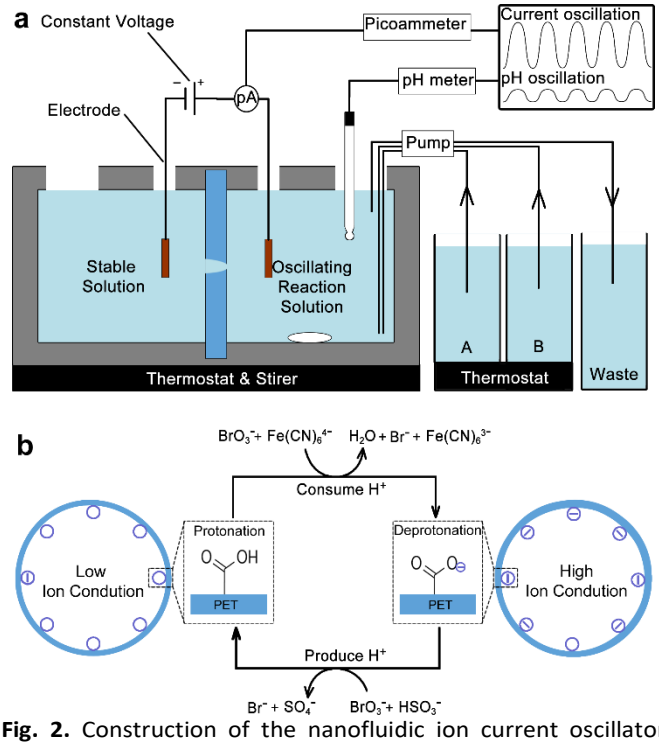

Fig. 2. Construction of the nanofluidic ion current oscillator system. (a) A schematic illustration of the experimental apparatus: a solution A of 0.065 M $NaBrO_3$ and a mixed solution B of 0.075 M Na_2SO_3, 0.02 M $K_4Fe(CN)_6$, and 0.01 M H_2SO_4 were pumped slowly into the cell on the channel tip side, while the cell on the base side was filled with stable reacted solution (pH 10, containing 0.065 M NaBr, 0.075 M Na_2SO_4, 0.02 M $K_3Fe(CN)_6$, and 0.01 M K_2SO_4). Volumes of solutions in both cells were 40 mL. Transmembrane ion current of the nanochannel was measured simultaneously with pH oscillation. (b) Autonomous and periodic switching of the

surface property of the nanochannel tip between lowly (left) and highly (right) charged states by the oscillatory reactions, thus realizing continuous oscillation of the nanochannel between low and high ion-conduction states.

Experimental setup for the oscillatory nanofluidic device is presented in Fig. 2a. The single nanochannel membrane was mounted in two halves of an electrochemical cell. Oscillating reactions were implemented in a continuously-fed stirred tank reactor arrangement, in which a solution A of $NaBrO_3$ and a mixed solution B of Na_2SO_3, $K_4Fe(CN)_6$, and H_2SO_4 were pumped slowly by peristaltic pumps into the reactor on the tip side of the nanochannel. Initial mixtures in the cell of tip side: V = 40 mL; $[NaBrO_3]_0$ = 0.065 M; $[Na_2SO_3]_0$ = 0.075 M; $[K_4Fe(CN)_6]_0$ = 0.02 M; $[H_2SO_4]_0$ = 0.01 M; $k_0 = 5.47 \times 10^{-4}$ s^{-1}. The input rates of solutions A and B were about 1.37×10^{-2} $mL \cdot s^{-1}$, output rate of the mixed reaction solution was 2.74×10^{-2} $mL \cdot s^{-1}$, and the stirring rate was 625 rpm. The cell on the base side was filled with 40 mL reacted solution (pH 10) consisting of 0.065 M NaBr, 0.075 M Na_2SO_4, 0.02 M $K_3Fe(CN)_6$, and 0.01 M K_2SO_4. The stable solution had same ion concentration and conductivity as the oscillating reaction solution. The working temperature was well controlled by a thermostat.

As shown in Fig. 2b, the oscillatory pH system which contained two primary composite reactions was coupled to the surface property changes of tip region of the nanochannel. One reaction produces H^+ in an autocatalytic fashion (Equation 1), while the other consumes H^+ in a slow process that produces an appropriate time lag (Equation 2).[45, 52] The carboxylate groups on the tip region could be protonated by the H^+-producing reaction, forming low ion-conduction state of the channel (Fig. 2b, left). Subsequently, the protonated carboxylate groups were deprotonated by the H^+-consuming process, and the channel became highly and negatively charged, leading to a high ion-conduction state (Fig. 2b, right). Therefore, the ion conduction of the nanochannel could be switched autonomously and cyclically by the oscillatory pH system.

$$BrO_3^- + 3HSO_3^- \rightarrow 3SO_4^{2-} + Br^- + 3H^+ \quad (1)$$

$$BrO_3^- + 6Fe(CN)_6^{4-} + 6H^+ \rightarrow 6Fe(CN)_6^{3-} + Br^- + 3H_2O \quad (2)$$

Based on above experimental conditions, the autonomous pH oscillation of the continuously-fed reacting solution on the tip side was measured by a pH meter, while the ion conductance oscillation of the nanofluidic system was characterized by measuring transmembrane ion current of the nanochannel with a picoammeter under a constant voltage. Time interval of the picoammeter for ion current measurement was set as 1 s, while time interval for the pH meter was 5 s. Fig. 3a shows a smooth pH-time curve observed experimentally by the pH meter, which exhibits a broad pH oscillation of the reacting solution from ca. 4.2 to ca. 6.6 at 40 °C. The pH oscillation period was approximately 1070 s and the pH amplitude was about 2.4. Fig. 3b shows current-time curve of the nanochannel measured by the picoammeter at +2 V, which demonstrates a periodic high-low switching behavior of the transmembrane ion current of the nanochannel. The period and full amplitude of ion current oscillation were about 1070 s and 1.8 nA, respectively, which well demonstrated that the ion current of the nanochannel oscillated simultaneously with the pH oscillation of the reaction solution. Compared with the un-continuous ion current switching of the nanochannel triggered by manually-supplied external pH stimuli (Fig. S4 in ESI), the ion current switching of the oscillatory nanofluidic system is autonomous, continuous, and periodic. Different from the nanoprecipitation-assisted transient ion current oscillations[60, 61] in single conical nanochannels, this novel nanofluidic oscillator could directly convert the chemical energy to ion-conduction oscillations.

After observation of ion current, the ion conductance (G) of the nanochannel could be experimentally observed from dividing the experimental ion current (I) by the applied voltage (U = 2 V): $G = I/U$. Fig. 4a (black line) shows oscillation of the experimental ion conductance value of the nanochannel. Besides, the ion conductance value of the uncharged bullet-shaped nanochannel could be theoretically described as a function of the conductivity (k) of the reaction solution (equation 3, see equations S1-S3 and Fig. S5 in ESI for detailed discussion).

$$G_{th} = f(k) = 1.27\ (nm) \times k\ (S.m^{-1}) \quad (3)$$

In order to further study the impact of the conductivity of the reaction solution on the ion-conduction oscillation of the nanochannel, we systematically measured conductivity, temperature, and redox potential changes of the reaction solution simultaneously with pH. As illustrated in Fig. S6 in ESI, the redox potential of the solution autonomously oscillated between 177 and 187 mV, and its period was similar to the pH oscillation. The solution temperature oscillated frequently but slightly between 39.2 and 40 °C, and its oscillation frequency was twice faster than pH's. The ion conductivity of the reacting solution fluctuated and increased slightly from 1.12 to 1.15 $S.m^{-1}$ (Fig. 4b), which did not oscillate periodically because it was a combination result of the ion-concentration oscillation and temperature oscillation of the reaction solution. Based on

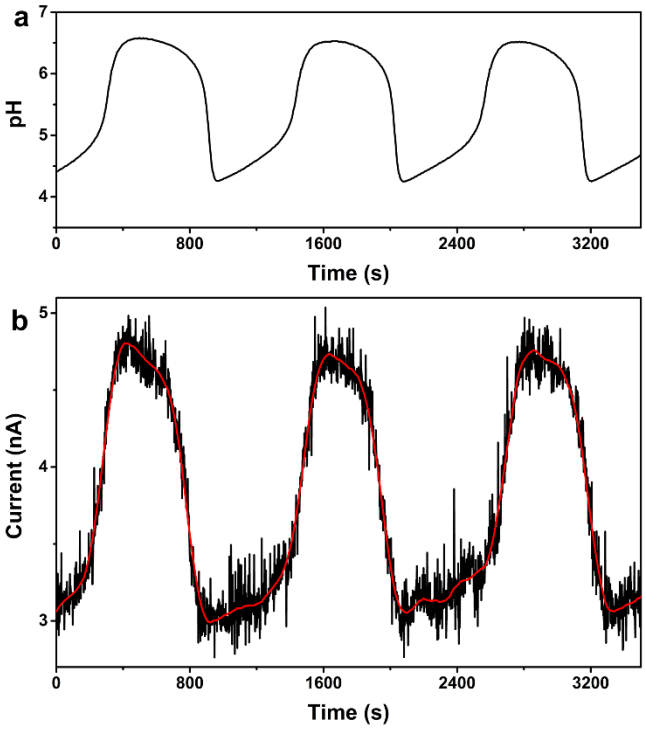

Fig. 3. Measurements of the nanofluidic oscillator. (a) Autonomous pH oscillation of the reacting solution on the tip side of the nanochannel between 4.2 and 6.6 measured by the pH meter at 40 °C. (b) Continuous and periodic ion current

oscillation of the nanochannel measured under a constantly applied voltage of +2 V. Red line was smoothed values of the ion currents. The ion current of the nanochannel oscillated simultaneously with the pH oscillation.

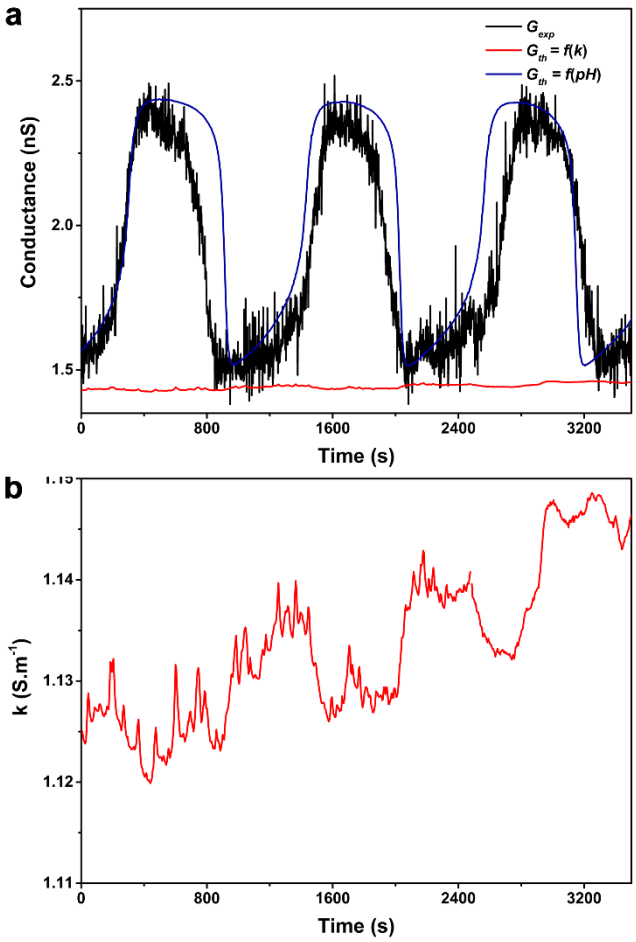

Fig. 4. Experimental and theoretical ion-conductance oscillations of the nanofluidic oscillator. (a) The experimental ion-conductance (G_{exp}) of the nanochannel oscillated simultaneously with pH (black line), the theoretical ion-conductance oscillation induced by the conductivity fluctuation (b) of the reaction solution (G_{th} = f(k), red line), and the theoretical ion-conductance oscillation expected from the pH oscillations in Fig. 2a using the titration data from Fig. S7 in ESI (G_{th} = f(pH), blue line). The measured ion-conductance values (black line) roughly agreed with the calculated values (blue line), but the conductivity fluctuation could not induce obvious changes of the ion conduction of the nanochannel (red line). (b) Conductivity fluctuation of the continuously-fed reaction solution measured by the conductivity meter at 40 °C.

the experimental conductivity variation in Fig. 4b, theoretical conductance change induced by the conductivity variation could be calculated from equation 3. As shown in Fig. 4a (red line), no obvious change of the channel conductance was obtained. Also indicated in Fig. 4a (blue line, G_{th} = f(pH)) is the theoretical ion-conduction oscillations calculated from the titration curve in Fig. S7 in ESI on the basis of the pH oscillations in Fig. 3a. Obviously, the theoretical ion-conduction oscillation is consistent with the experimental result. Therefore, autonomous pH oscillation of the reaction solution was the key factor for ion current oscillation of the nanofluidic system.

We further conducted an experiment of measuring ion current oscillations of the nanofluidic oscillator at various temperatures from 30 to 45 °C because the temperature has been reported as one of the key factors that affect the periods and amplitudes of pH oscillators.[59] As shown in Fig. 5, the periods of both pH and ion-current oscillations decreased gradually with increasing the working temperature. Oscillation periods of both pH and ion current were ~2200 s at 30 °C, ~1630 s at 35 °C, ~1070 s at 40 °C, and ~585 s at 45 °C, respectively. However, the amplitudes of pH oscillations at different temperatures maintained around 2.4. Amplitudes of ion-current oscillations were ~2.0 nA at 30 °C, ~2.2 nA at 35 °C, ~1.2 nA at 40 °C, and ~1.0 nA at 45 °C, respectively. Therefore, the nanofluidic oscillators had temperature-dependent periods and amplitudes of ion current oscillations.

It is also worth noting that the noise of the ion current observed in the nanofluidic oscillator system is much higher than the previously reported ion current noises of single nanochannels measured in stable electrolyte solutions.[62-64] Moreover, the noise frequency of the current oscillator increased with the working temperature increasing (Fig. 3a, 3b, and 3d), which could be attributed to the temperature-increased fluctuations in surface charges of the nanochannels and thermal fluctuations in the conductivity of the solutions.[63] Besides, after done a series of contrast experiments, we found that the peristaltic pump used in the nanofluidic oscillator system was the main reason that caused the high ion current noise of the nanofluidic oscillator. The noise could be reduced by shutting down the peristaltic pump (Fig. S8 in ESI). Therefore, in order to avoid the influence of the peristaltic pump, future nanofluidic oscillators with low ion current noise can be developed based on closed oscillatory pH systems[65, 66] which do not need peristaltic pumps to feed reacting solution into the reactor. In addition, through comparing current curves (in Fig.s 2b and 3c) measured under time interval of 1 s and current curves (Fig.s 3a, 3b, and 3d) measured under time interval of 5 s, we found that the ion current noise could be reduced by increasing time interval for ion current measurement.

Conclusions

In summary, we have described the construction of oscillatory nanofluidic devices based on the single nanochannel and the chemical oscillator. An oscillatory pH oscillator ($NaBrO_3$-Na_2SO_3-$K_4Fe(CN)_6$-H_2SO_4) was incorporated into the single bullet-shaped nanochannel to be the energy source for periodically switching the nanochannel between low and high ion-conduction states. The oscillating-reaction-driven nanofluidic system exhibited novel autonomous, periodic and continuous ion current properties under the continuously-supplied constant reacting solution. Experimental results also demonstrated that the oscillation period of the nanofluidic oscillator decreased gradually with the working temperature increasing. Further variation of the oscillatory nanofluidic devices could be achieved by integrating different artificial nanochannels with diverse oscillating chemical reactions. This successful study is a potential step toward the ability to directly covert chemical energy to ion-conduction oscillation in nanofluidics and to simulate the oscillation behaviors in living

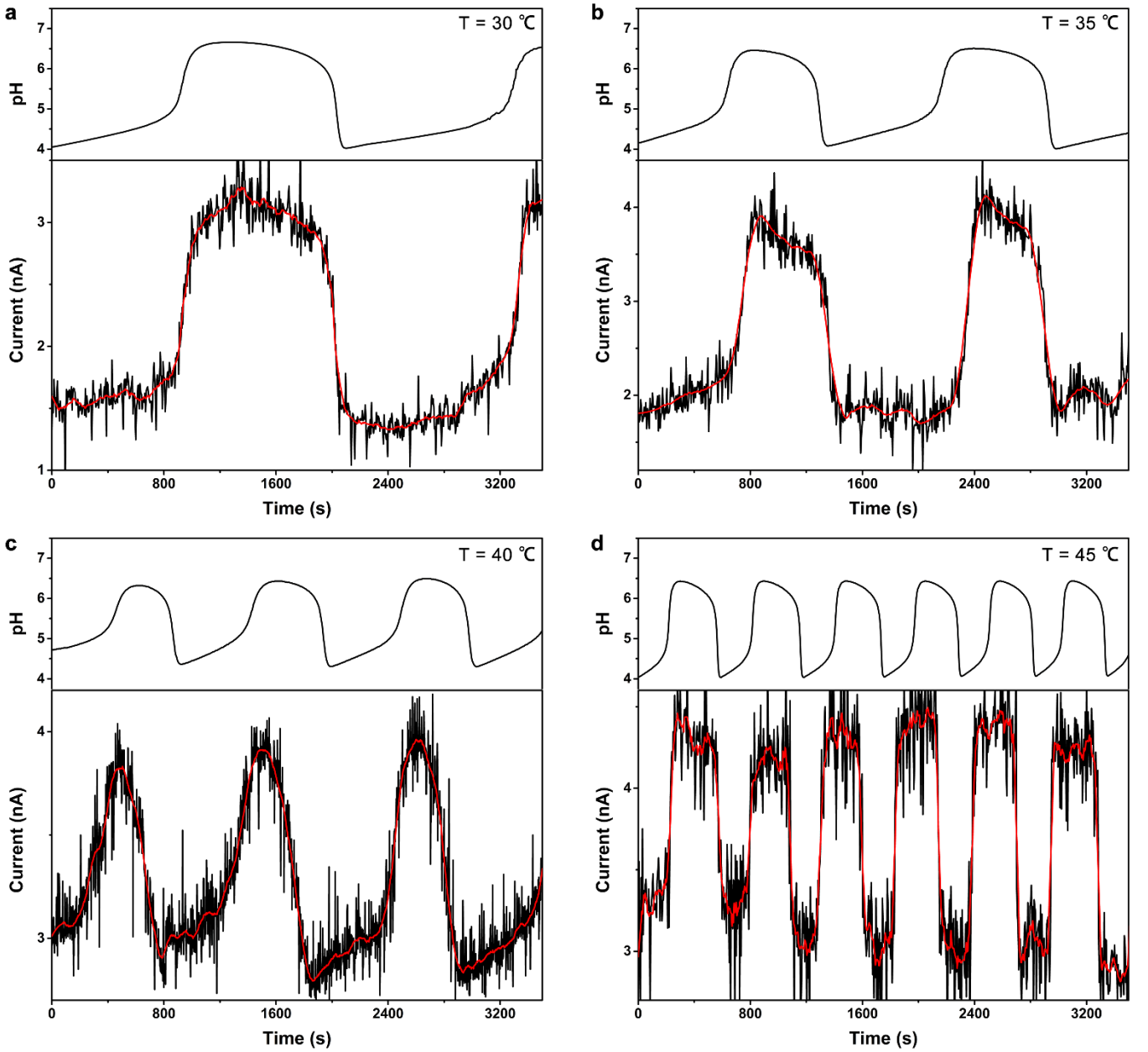

Fig. 5. Temperature-dependent pH and ion current oscillations of the nanofluidic oscillator system: (a) 30 °C and, (b) 35 °C, (c) 40 °C, (d) 45 °C. Oscillation periods of pH and ion current of the oscillator gradually decreased with increasing working temperature. Time interval of (a), (b), and (d) was 5 s, respectively, while time interval of (c) was 1 s. The applied voltage for ion current measurements was +2 V. Red lines were smoothed values of the ion currents

organisms. On the basis of these findings, we believe that artificial oscillatory nanofluidic systems offer real promise for preparing periodic mass-delivery devices that could be employed in closed environments.

Experimental section

Materials. The ion-tracked PET membranes were purchased from GSI (Darmstadt, Germany). Potassium hexacyanoferrate (II) trihydrate ($K_4Fe(CN)_6$, 98.5%-102.0%) was purchased from Sigma-Aldrich. Sodium bromate ($NaBrO_3$, 99.5%) and sodium sulfite (Na_2SO_3, 98%) were purchased from Alfa Aesar (China). Potassium chloride (KCl, 99.8%), potassium hydroxide (KOH, 98.0%), sulfuric acid (H_2SO_4, 95.0%-98.0%), and sodium hydroxide (NaOH, 96.0%) were purchased from Sinopharm Chemical Reagent Beijing (China). Formic acid (HCOOH, ≥ 88%), and hydrochloric acid (HCl, 36.0%-38.0 %) were purchased from Beijing Chemical Works (China).

Fabrication of single bullet-shaped nanochannels. The single bullet-shaped nanochannels investigated in this work were fabricated in 12 μm thick PET membranes by adopting the method of surfactant-protected ion-track-etching.[14, 58] One side of the membrane was etched by 6 M NaOH + 0.025% sodium dodecyl diphenyloxide disulfonate, while the other side was etched by 6 M NaOH. During the etching process, a constant voltage of 1.0 V was applied across the film. After

etching for about 3-4 minutes, a 1 M KCl + 1 M HCOOH solution that is able to neutralize the etchant was added into the containers on both sides of the membrane, thus slowing down and finally stopping the etching process, and single bullet-shaped nanochannels were produced in the PET membranes. The nanochannel membranes were then soaked in MilliQ water (18.2 MΩ) to remove residual salts.

SEM characterization. SEM measurements were taken in the field-emission mode using a FEI Magellan 400 extreme high resolution microscope at an acceleration voltage of 5 kV. Surfaces of the nanochannel membranes were coated with an ultrathin layer of gold before characterization by SEM.

Electrochmical measurement. Ion current measurements were carried out by a Keithley 6487 picoammeter (Keithley Instruments, Cleveland, OH). Pt electrodes were used to apply transmembrane potentials across the nanochannel membranes. The cathode faced the base side of the nanochannel, while the anode faced the tip side of the nanochannel. The oscillatory ion transport behavior of the nanofluidic oscillator was measured under a constant condition: the tip side was continuously fed with reacting solution, while the base side was contacted with a stable solution (Fig. 1b). The stable solution was firstly prepared by mixing 20 mL solution A with 20 mL solution B. The pH value of the un-fed mixed solution was initially decreased and then increased, finally reached a stable value of ca. 10 after reaction for 3h (Fig. S6 in ESI). After added the reacted 40 mL mixed solution into the base side of the nanochannel (Fig. 1b, left), solution A and solution B was continuously fed into the tip side of the nanochannel by peristaltic pumps (Fig. 1b, right). Different from pH value of the un-fed mixed solution, pH value of the continuously-fed reacting solution autonomously oscillated. The pH value, redox potential, and ion conductivity of the reacting solution was measured by a Mettler SevenExcellence pH/mV/Conductivity meter. As shown in Fig. S7 in the Supporting Information, pH of initial mixed reaction solution is above 7 and the pH oscillated between 4.2 and 6.6 after the first H^+-producing process.The ion current measurement was started when the pH oscillation of the reaction solution was stabilized.

Acknowledgements

This research is supported by the Australian Research Council (DE170100006, DP150100765) and the National Natural Science Foundation (21501185). The authors thank the Material Science Group of GSI (Darmstadt, Germany) for providing the ion-irradiated samples and the staff of Monash Centre for Electron Microscopy at Monash University for their technical assistance with SEM.

Notes and references

1 S. W. Kowalczyk, T. R. Blosser and C. Dekker, *Trend. Biotechnol.*, 2011, **29**, 607.
2 H. Zhang, Y. Tian and L. Jiang, *Chem. Commun.*, 2013, **49**, 10048.
3 X. Hou, W. Guo and L. Jiang, *Chem. Soc. Rev.*, 2011, **40**, 2385.
4 H. Zhang, Y. Tian and L. Jiang, *Nano Today*, 2016, **11**, 61.
5 G. Perez-Mitta, A. G. Albesa, C. Trautmann, M. E. Toimil-Molares and O. Azzaroni, *Chem. Sci.*, 2017, **8**, 890.
6 B. Hille, *Ion Channels of Excitable Membranes*, Sinauer Associates, Sunderland, Massachusetts, , 3rd edn., 2001.
7 A. de la Escosura-Muñiz and A. Merkoçi, *ACS Nano*, 2012, **6**, 7556.
8 M. Tagliazucchi and I. Szleifer, *Soft Matter*, 2012.
9 B. N. Miles, A. P. Ivanov, K. A. Wilson, F. Dogan, D. Japrung and J. B. Edel, *Chem. Soc. Rev.*, 2013, **42**, 15.
10 Y. X. Shen, P. O. Saboe, I. T. Sines, M. Erbakan and M. Kumar, *J. Membrane Sci.*, 2014, **454**, 359.
11 Z. Siwy, P. Apel, D. Baur, D. D. Dobrev, Y. E. Korchev, R. Neumann, R. Spohr, C. Trautmann and K.-O. Voss, *Surf. Sci.*, 2003, **532–535**, 1061.
12 F. Xia, W. Guo, Y. Mao, X. Hou, J. Xue, H. Xia, L. Wang, Y. Song, H. Ji, Q. Ouyang, Y. Wang and L. Jiang, *J. Am. Chem. Soc.* , 2008, **130**, 8345.
13 B. Yameen, M. Ali, R. Neumann, W. Ensinger, W. Knoll and O. Azzaroni, *Nano Lett.*, 2009, **9**, 2788.
14 H. Zhang, X. Hou, L. Zeng, F. Yang, L. Li, D. Yan, Y. Tian and L. Jiang, *J. Am. Chem. Soc.*, 2013, **135**, 16102.
15 X. Hou, Y. Liu, H. Dong, F. Yang, L. Li and L. Jiang, *Adv. Mater.*, 2010, **22**, 2440.
16 H. Zhang, Y. Tian, J. Hou, X. Hou, G. Hou, R. Ou, H. Wang and L. Jiang, *ACS Nano*, 2015, **9**, 12264.
17 M. Ali, P. Ramirez, S. Mafé, R. Neumann and W. Ensinger, *ACS Nano*, 2009, **3**, 603.
18 G. Perez-Mitta, L. Burr, J. S. Tuninetti, C. Trautmann, M. E. Toimil-Molares and O. Azzaroni, *Nanoscale*, 2016, **8**, 1470.
19 F. M. Gilles, M. Tagliazucchi, O. Azzaroni and I. Szleifer, *J. Phys. Chem. C*, 2016, **120**, 4789.
20 G. Perez-Mitta, W. A. A. Marmisollé, C. Trautmann, M. E. Toimil-Molares and O. Azzaroni, *J. Am. Chem. Soc.*, 2015, **137**, 15382.
21 B. Yameen, M. Ali, R. Neumann, W. Ensinger, W. Knoll and O. Azzaroni, *Chem. Commun.*, 2010, **46**, 1908.
22 B. Yameen, M. Ali, R. Neumann, W. Ensinger, W. Knoll and O. Azzaroni, *J. Am. Chem. Soc.*, 2009, **131**, 2070.
23 B. Yameen, M. Ali, R. Neumann, W. Ensinger, W. Knoll and O. Azzaroni, *Small*, 2009, **5**, 1287.
24 L. X. Zhang, S. L. Cai, Y. B. Zheng, X. H. Cao and Y. Q. Li, *Adv. Funct. Mater.*, 2011, **21**, 2103.
25 Y. Zhou, W. Guo, J. Cheng, Y. Liu, J. Li and L. Jiang, *Adv. Mater.*, 2012, **24**, 962.
26 M. Ali, S. Nasir, P. Ramirez, I. Ahmed, Q. H. Nguyen, L. Fruk, S. Mafe and W. Ensinger, *Adv. Funct. Mater.*, 2012, **22**, 390.
27 Q. Zhang, Z. Liu, K. Wang and J. Zhai, *Adv. Funct. Mater.*, 2015, **25**, 2091.
28 M. R. Powell, L. Cleary, M. Davenport, K. J. Shea and Z. S. Siwy, *Nat. Nanotechnol.*, 2011, **6**, 798.
29 S. F. Buchsbaum, G. Nguyen, S. Howorka and Z. S. Siwy, *J. Am. Chem. Soc.*, 2014, **136**, 9902.
30 W. J. Lan, D. A. Holden and H. S. White, *J. Am. Chem. Soc.*, 2011, **133**, 13300.
31 M. Ali, Q. H. Nguyen, R. Neumann and W. Ensinger, *Chem. Commun.*, 2010, **46**, 6690.
32 Y. L. Xu, X. Sui, S. Guan, J. Zhai and L. C. Gao, *Adv. Mater.*, 2015, **27**, 1851.
33 W. Guo, F. Hong, N. Liu, J. Huang, B. Wang, R. Duan, X. Lou and F. Xia, *Adv. Mater.*, 2015, **27**, 2090.
34 M. Ali, I. Ahmed, S. Nasir, P. Ramirez, C. M. Niemeyer, S. Mafe and W. Ensinger, *ACS Applied Mater. Interfaces*, 2015, **7**, 19541.

35 R. Fang, H. Zhang, L. Yang, H. Wang, Y. Tian, X. Zhang and L. Jiang, *J. Am. Chem. Soc.*, 2016, **138**, 16372.
36 G. Perez-Mitta, A. G. Albesa, W. Knoll, C. Trautmann, M. E. Toimil-Molares and O. Azzaroni, *Nanoscale*, 2015, **7**, 15594.
37 M. Liu, H. Zhang, K. Li, L. Heng, S. Wang, Y. Tian and L. Jiang, *Adv. Funct. Mater.*, 2015, **25**, 421.
38 Q. Liu, K. Xiao, L. Wen, H. Lu, Y. Liu, X. Y. Kong, G. Xie, Z. Zhang, Z. Bo and L. Jiang, *J. Am. Chem. Soc.*, 2015, **137**, 11976.
39 F. Zhang, J. Ma, Y. Sun, I. Boussouar, D. Tian, H. Li and L. Jiang, *Chem. Sci.*, 2016, **7**, 3227.
40 K. Raidongia and J. Huang, *J. Am. Chem. Soc.*, 2012, **134**, 16528.
41 S. Rao, S. Lu, Z. Guo, Y. Li, D. Chen and Y. Xiang, *Adv. Mater.*, 2014, **26**, 5846.
42 D. G. Haywood, A. Saha-Shah, L. A. Baker and S. C. Jacobson, *Anal. Chem.*, 2015, **87**, 172.
43 B. Novak and J. J. Tyson, *Nat. Rev. Mol. Cell. Biol.*, 2008, **9**, 981.
44 J. R. Kim, D. Shin, S. H. Jung, P. Heslop Harrison and K. H. Cho, *J. Cell Sci.*, 2010, **123**, 537.
45 M. Orban, K. Kurin-Csorgei and I. R. Epstein, *Acc. Chem. Res.*, 2015, **48**, 593.
46 R. Yoshida, *Adv. Mater.*, 2010, **22**, 3463.
47 J. R. Howse, P. Topham, C. J. Crook, A. J. Gleeson, W. Bras, R. A. L. Jones and A. J. Ryan, *Nano Lett.*, 2006, **6**, 73.
48 S. Maeda, Y. Hara, R. Yoshida and S. Hashimoto, *Macromol. Rapid Commun.*, 2008, **29**, 401.
49 H. Nakagawa, Y. Hara, S. Maeda and S. Hasimoto, *Polymers*, 2011, **3**, 405.
50 R. Yoshida and Y. Murase, *Colloid. Surf. B Biointerfaces*, 2012, **99**, 60.
51 G. P. Misra and R. A. Siegel, *J. Controlled Release*, 2002, **79**, 293.
52 E. Tian, Y. Ma, L. Cui, J. Wang, Y. Song and L. Jiang, *Macromol. Rapid Commun.*, 2009, **30**, 1719.
53 X. J. Qi, C. H. Lu, X. Liu, S. Shimron, H. Yang and I. Willner, *Nano Lett.*, 2013, **13**, 4920.
54 I. Lagzi, B. Kowalczyk, D. Wang and B. A. Grzybowski, *Angew. Chem. Int. Ed.*, 2010, **49**, 8616.
55 T. Masuda, M. Hidaka, Y. Murase, A. M. Akimoto, K. Nagase, T. Okano and R. Yoshida, *Angew. Chem. Int. Ed.*, 2013, **52**, 7468.
56 J. Wang, R. Fang, J. Hou, H. Zhang, Y. Tian, H. Wang and L. Jiang, *ACS Nano*, 2017, **11**, 3022.
57 Z. Siwy and A. Fulinski, *Phys. Rev. Lett.*, 2002, **89**, 198103.
58 P. Y. Apel, I. V. Blonskaya, O. L. Orelovitch, P. Ramirez and B. A. Sartowska, *Nanotechnology*, 2011, **22**, 175302.
59 E. C. Edblom, Y. Luo, M. Orban, K. Kustin and I. R. Epstein, *J. Phys. Chem.*, 1989, **93**, 2722.
60 M. R. Powell, M. Sullivan, I. Vlassiouk, D. Constantin, O. Sudre, C. C. Martens, R. S. Eisenberg and Z. S. Siwy, *Nat. Nanotech.*, 2008, **3**, 51.
61 L. Innes, M. R. Powell, I. Vlassiouk, C. Martens and Z. S. Siwy, *J. Phys. Chem. C*, 2010, **114**, 8126.
62 Z. Siwy and A. Fuliński, *Phys. Rev. Lett.*, 2002, **89**, 158101.
63 M. R. Powell, C. Martens and Z. S. Siwy, *Chem. Phys.*, 2010, **375**, 529.
64 B. Hyland, Z. S. Siwy and C. C. Martens, *J. Phys. Chem. Lett.*, 2015, **6**, 1800.
65 E. Poros, V. Horváth, K. Kurin-Csörgei, I. R. Epstein and M. Orbán, *J. Am. Chem. Soc.*, 2011, **133**, 7174.
66 G. Rabai, *Phys. Chem. Chem. Phys.*, 2011, **13**, 13604.